DOI: 10.1007/s12541-010-0121-1

Bubble Actuation by Electrowetting-on-Dielectric (EWOD) and Its Applications: A Review

Sang Kug Chung[1,#], Kyehan Rhee[1] and Sung Kwon Cho[2]

1 Department of Mechanical Engineering, Myongji University, San 38-2 Namdong, Cheoin-Gu, Yongin, Gyeonggido, South Korea, 449-728
2 Department of Mechanical Engineering and Materials Science, University of Pittsburgh, Pittsburgh, PA, USA, 15261
Corresponding Author / E-mail: skchung@mju.ac.kr, TEL: +82-31-330-6346, FAX: +82-31-321-4959

KEYWORDS: Microfluidics, Lab-on-a-chip, Bubble dynamics, Cavitational microstreaming

This paper reviews the principles, operations, and applications of bubble-based electrowetting-on-dielectric (EWOD). EWOD has proved to be an efficient tool in digital microfluidics that employs discrete droplets, and various applications that use the principles of EWOD have been developed from lab-on-a-chip to optical systems. Similar to its use with droplets, EWOD can also be applied to gaseous bubbles. This review begins with a discussion of the principles of EWOD for a bubble on an electrode covered with a hydrophobic dielectric layer. It then addresses EWOD actuation and the transportation of a bubble in an aqueous medium, along with a physical explanation of bubble motion. The operation of EWOD is then extended to the on-chip creation/elimination and splitting of bubbles. In particular, micro-mixers and pumps are discussed as potential applications of these operations. Unlike droplets, bubbles can be easily oscillated by external excitation, which provides additional functionalities. By integrating EWOD with external excitation, a number of new advanced applications are introduced, including the capture/separation of particles and the propulsion of objects. In these advanced operations, cavitational microstreaming flows and acoustic radiation forces are mainly responsible for the physical mechanisms. This paper also discusses these advanced operations along with their underlying physics. It is expected that in addition to bubble oscillation, other bubble actuation modes will create new functionalities and new potential applications.

Manuscript received: August 23, 2010 / Accepted: October 18, 2010

NOMENCLATURE

ρ = fluid density
μ = fluid dynamic viscosity
V = mean fluid velocity
L = characteristic length
θ = contact angle under an applied electrical potential
θ_e = equilibrium contact angle
V = electrical potential
ε = permittivity of a dielectric layer
γ = interfacial tension
t = thickness of a dielectric layer
θ_R = contact angle on the right side of a bubble
θ_L = contact angle on the left side of a bubble
θ_{adv} = advancing contact angle
θ_{rec} = receding contact angle
w = width of a bubble base
R = radius of a bubble
$F_{driving}$ = bubble driving force
ψ = streaming function of a cavitational streaming flow
ε = amplitude of bubble oscillation normalized by a radius of a bubble
ω = angular frequency of an applied acoustic wave
r = distance from a bubble center
$\Delta\phi$ = phase shift between volume and translational oscillations

1. Introduction

As interest grows in biomedical and genomics applications such as DNA sequencing, microarrays, and bio-entity manipulation, lab-

on-a-chip or micro total analysis systems (μTAS) technologies becomes increasingly important.[1-7] A lab-on-a-chip is a small device made up of microfluidic components such as channels, pumps, valves, and sensors on a microscale; the use of such devices permits the realization of many biological/chemical laboratory functions on a single chip. The key research topic in the development of these systems is microfluidics, which deals with fluids on a submicroliter scale or even smaller volumes.

In dealing with such small volumes, fluid manipulation techniques that are different from those used on a macroscale become necessary, because important physical parameters in the system can be different.[8,9] From the point view of fluid mechanics, the Reynolds number (Re = $\rho VL/\mu$, where ρ, V, L, μ are the density, mean velocity, characteristic length, and dynamic viscosity of a fluid, respectively), a dimensionless number that shows the ratio of inertia forces to viscous forces under given flow conditions, is most commonly used as a reference parameter to identify the dominant governing forces and to characterize flows. As the size of a flow system decreases, the Reynolds number linearly decreases and the viscous forces become more dominant. As a consequence, the fluid pumping techniques commonly used in macrochannels (e.g., pressure-driven pumping) may become inefficient for driving fluid plugs in microchannels (which have low Reynolds number flows) because of the extremely high resistance generated by the viscous forces.

As alternatives, a variety of microfluidic manipulation technologies has been developed that are mainly based on capillary forces and electrokinetic methods such as electrophoresis, electroosmosis, dielectrophoresis, and others.[10-17] Electrowetting-on-dielectric (EWOD),[2,3,7,18-20] which is another of these microfluidic manipulation methods for microscale applications, has a distinct feature, namely that the microfluidic operations are carried out in the form of discrete fluids (most commonly, droplets) without channel networks. This is fundamentally different from other existing methods that make use of complicated microchannels. Microfluidics based on EWOD thus offers outstanding advantages such as its use of extremely small fluid volumes, low power consumption, and rapid response time. Thanks to these advantages, various applications using the principles of EWOD have been developed: lab-on-a-chips,[2,4,21] electrical switches,[17,22-24] liquid lens,[25-27] microprism arrays,[28,29] electrowetting displays,[30-32] and others.[33-40]

In the abovementioned applications, the target fluids are mainly liquid. Accordingly, the focus of many review papers on EWOD has been on the dynamics of liquid EWOD. Recently, however, it has been found that gaseous bubbles can also be efficiently manipulated using EWOD, a discovery that has spawned many useful applications. This paper reviews the dynamics of EWOD with bubbles along with its applications, which include the manipulation and propulsion of micro-objects. In particular, as discussed in the sections on applications, it is interesting to see how EWOD has been integrated with other fluidic manipulation principles such as microstreaming and acoustic radiation with bubbles (gas/liquid interfaces).

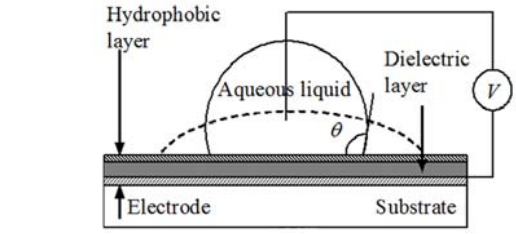

(a)

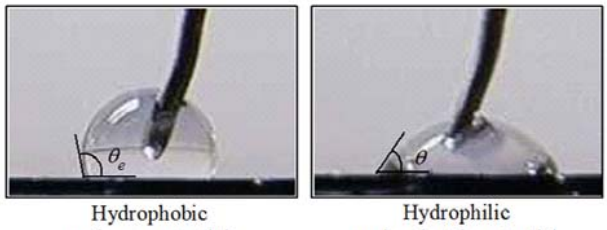

(b)

Fig. 1 Principle of electrowetting on dielectric: (a) Schematic configuration; (b) Pictures of basic electrowetting demonstration on a sessile drop. Reproduced with permission[3] (© 2003 IEEE)

2. Theoretical Background

2.1 Electrowetting-on-Dielectric (EWOD)

About a hundred years ago, Gabriel Lippmann,[41] a French physicist, first discovered the electrocapillary phenomenon in which the interfacial tension of mercury in an electrolyte solution could be modified by applying electrical voltages between the mercury and the solution. Though he invented a few applications based on this principle, the electrolysis caused by the flow of electric current through electrolyte solutions, even if it was under a few hundred millivolts, presented an obstacle to a wide range of possible applications. A century later, this principle is now drawing considerable attention with the emergence of new microfabrication technologies.

Berge et al.[42,43] performed a sessile water droplet test on an electrode covered with a thin hydrophobic dielectric layer to prevent electrolysis and found that the interfacial tension between the droplet and solid surface could be efficiently modified by applying voltages between the electrode and the droplet, as shown in Fig. 1. This process is called electrowetting, or to be precise, electrowetting-on-dielectric (EWOD). When voltages are applied between the droplet and electrode (that is, across the dielectric layer), the dielectric layer acts as a capacitor, so that electric charge layers are built up near the solid-liquid interfaces in the dielectric layer with a minimal flow of electric current. The thermodynamic interpretation of this is that the lowered surface energy generated because of the charge buildup causes the droplet to spread out on the dielectric layer because the electric charges around the three-phase contact line (TCL) are accumulated by the applied electric potentials. As a consequence, the applied voltages control the wettability of the dielectric surface. EWOD has demonstrated excellent reversibility and robust operation because it involves no mechanical movement of solid parts.[7,18]

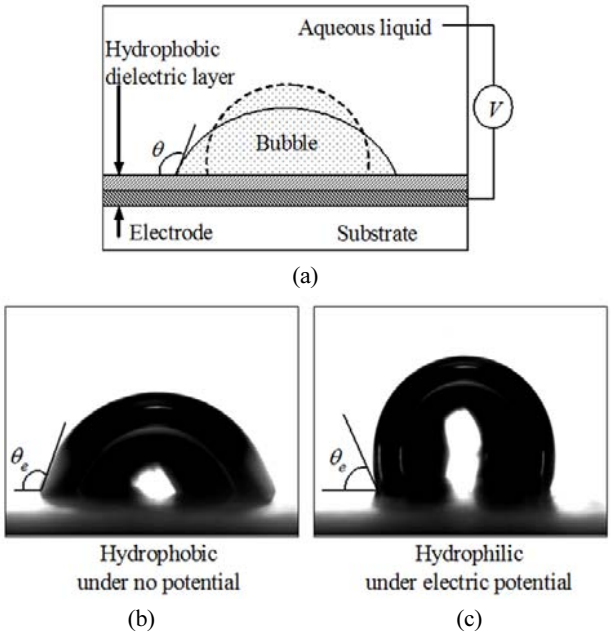

Fig. 2 Preliminary results of electrowetting principle with an air bubble. The bubble retracts under electric potential and reversibly spreads back to the initial state under no electric potential: (a) configuration; (b) no electric potential applied; (c) electric potential applied. Reprinted with permission[19]

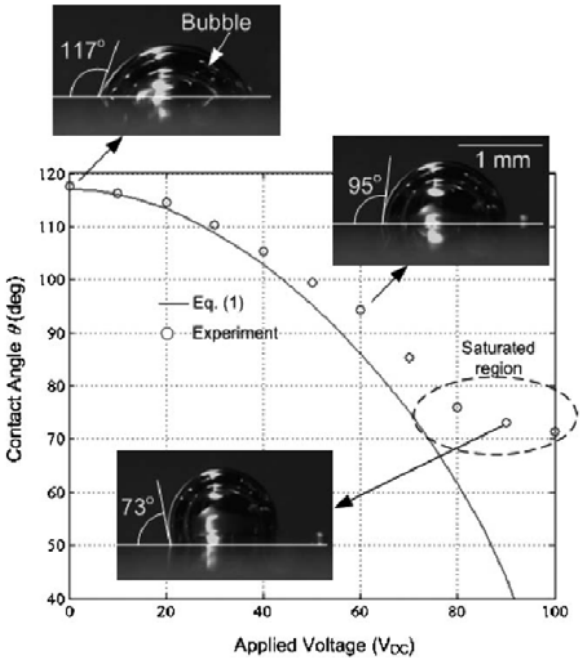

Fig. 3 Contact angle measurement in a capped bubble (volume ~ 1 μL) under EWOD. As the applied voltage increases, the contact angle decreases and as a result the bubble contracts. Over about 80 V_{DC}, the contact angle is saturated. The insets show the side view at the corresponding contact angle. Reprinted with permission[47]

The relationship between the applied voltages and the change in contact angle, which is given by the so-called Lippmann-Young equation, can be derived from the minimum free-energy requirement for thermodynamic equilibrium conditions as follows:

$$\cos\theta = \cos\theta_e + \frac{\varepsilon V^2}{2\gamma t} \tag{1}$$

where θ is the contact angle under the externally applied electric potential V, θ_e is the equilibrium contact angle at V= 0 V, ε is the permittivity of the dielectric layer, γ is the interfacial tension between the droplet and the surrounding fluid, and t is the thickness of the dielectric layer. This equation shows that the cosine of the contact angle can be parabolically modulated by the applied electric potential. In many configurations of millimeter-sized droplets, the empirical results on contact angles have been successfully correlated to equation (1) within a moderate range of contact angles. Other theoretical approaches such as Maxwell stress analysis of electrostatic force[20,44] and an electromechanical framework[45,46] also confirmed equation (1).

For a non-conductive (more specifically, gaseous) fluid droplet in a fluid conducting medium—a medium which is opposite to that of a water droplet in an air or oil environment—the electrowetting principle is also applicable. Figure 2 shows that an air bubble in an aqueous environment is actuated by EWOD.[19,47,48] However, the bubble retracts under an electric potential due to the decrease in the contact angle. It should be noted that the contact angle is also defined on the aqueous liquid side (Fig. 2(a)). Zhao el al.[47,49] performed an EWOD experiment for a sessile air bubble in a DI water reservoir that consisted of four glass faces as the sides and a plane EWOD electrode on the bottom, as shown in Figs. 2 and 3.

The modification of the contact angle with respect to the applied voltages is in good agreement with the Lippmann-Young equation up to 80 V_{DC}. However, as shown in Fig. 3, the contact angle does not change beyond a certain critical voltage, even though higher voltages are applied, which is the same trend that is observed in the water droplet configuration. This phenomenon is called contact angle saturation in EWOD.[50-55] While several hypotheses have been advanced to explain it, it has yet to be clearly understood. For more details on this phenomenon, refer to other review articles.[2,7,18]

2.2 Droplet/Bubble Transportation by EWOD

As mentioned in the previous section, it is innovative to use the dielectric layer between the droplet and electrode. The introduction of the dielectric layer results in not only a large modification in the contact angle but also a reversible droplet operation with a minimized electrolysis problem. Another innovation in the development of EWOD is droplet transportation using patterned EWOD electrodes, as shown in Fig. 4. Pollack et al.[56-58] first demonstrated droplet transportation using conducting droplets ranging in size from several nanoliters to several microliters that were positioned between two glass plates. The bottom plate had addressable EWOD electrodes covered with dielectric and hydrophobic layers, whereas the top plate had a continuous ground electrode, as shown in Fig. 4. The conducting droplet immerged in oil was initially placed at the center of the bottom electrodes and was sandwiched between the two plates. When voltages were applied between the adjacent bottom and ground electrodes, the local contact angle on the side adjacent to the droplet changed according to the Lippmann-Young equation. Once the applied

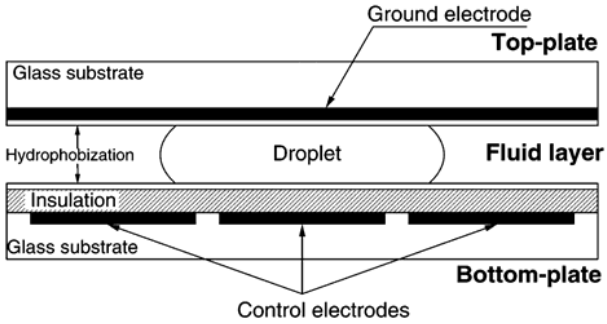

Fig. 4 Schematic cross-section of the electrowetting chip. Reprinted with permission[56]

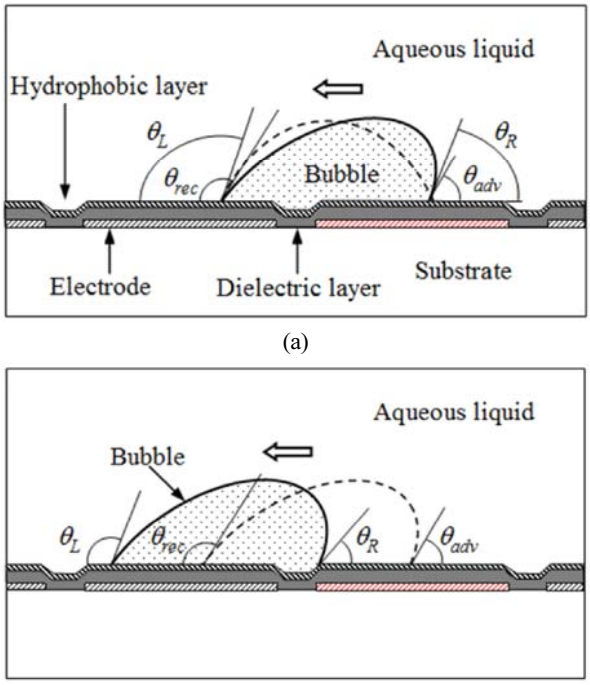

Fig. 5 Sequential sketches of bubble transportation: (a) Immediately after the first electrode on the right of the bubble is activated, the bubble is deformed but does not move since the contact angles (θ_L and θ_R) on the left and right sides of the bubble are still within the contact angle hysteresis range (i.e., $\theta_L < \theta_{rec}$ and $\theta_R > \theta_{adv}$ for the bubble); (b) Once the contact angles pass over the critical angles (θ_{adv} and θ_{rec}) by electrowetting, the bubble starts to move. Reprinted with permission[19]

voltages exceeded a certain threshold, the droplet moved to the adjacent activated electrode.

This work was the first demonstration of digital microfluidic lab-on-a-chip systems that used droplets instead of the continuous microfluidic systems.

Similar to the transportation of a droplet, an air bubble can also be transported on a two-dimensional surface by EWOD actuation. In order to move a bubble on a solid surface, the bubble needs to overcome the adhesion force caused by contact angle hysteresis.[22,59-61] Figure 5 shows macroscopic sketches of how a bubble placed over an array of electrodes behaves in response to electrowetting actuation and contact angle hysteresis.[19] As denoted by the broken line in Fig. 5(a), the bubble initially sits on a dielectric layer in such a way that the right side of the bubble is positioned over the second electrode from the right. Here, the contact angles on both sides of the bubble are equal to the equilibrium contact angle θ_e. The activation of the electrode on the right of the bubble would decrease the contact angle θ_R on the right side of the bubble according to the Lippmann-Young equation, whereas the contact angle θ_L on the left side of the bubble would increase slightly because of the deformation of the bubble. It should be noted that all the contact angles are referred to as the macroscopic apparent contact angle, not the microscopic intrinsic contact angle. The three-phase contact lines (TCL) on both the left and right sides of the bubble do not move, even though the bubble shape is deformed. As a result, the bubble manifests no sliding movement (Fig. 5(a)).

This lack of movement is due to contact angle hysteresis (the difference between θ_{adv} and θ_{rec}): in order for the TCL to advance or recede, the contact angle needs to pass beyond critical values (θ_{adv} and θ_{rec}) that are different from the equilibrium contact angle θ_e. These critical angles are referred to as the advancing contact angle θ_{adv} and the receding contact angle θ_{rec}. Many physical parameters could play a role in the occurrence of this phenomenon, such as the surface roughness and the degree of heterogeneity of the surface, among others. Only if the contact angle θ_R is lower than the advancing contact angle θ_{adv} and the contact angle θ_L is higher than the receding contact angle θ_{rec}, will the bubble begin to move to the left. These conditions require a large span of modulation of the contact angle by electrowetting actuation for the initiation of bubble motion.

By considering the static mechanical equilibrium,[59,62-64] the bubble driving force $F_{driving}$ produced by electrowetting actuation may be approximated as follows:

$$F_{driving} = 2\gamma w \sin\left(\frac{\theta_L + \theta_R}{2}\right)\left(\cos\theta_R - \cos\theta_L\right) \quad (2)$$

where γ is the interfacial tension between the liquid and the bubble, and w is the width of the bubble base that linearly scales with the radius R of the bubble. Here, the contact angle θ_R of the bubble is modulated by electrowetting actuation and decreases from the equilibrium contact angle θ_e with a large span (generally ~40°). Therefore, the sine term in Eq. (2) can be roughly approximated to the sine of the equilibrium contact angle θ_e, whereas the difference in the cosines in Eq. (2) increases as the contact angle θ_R for the bubble is decreased by electrowetting modulation. Based on these relationships, it can be concluded that the maximum driving force can be achieved when the equilibrium contact angle is close to 90° and the contact angle modulation is maximized by electrowetting actuation. This force can be in the micronewton range. For example, when θ_R = 60° and θ_L = 120° with an air bubble of 10 μm diameter in water, the driving force is estimated to be roughly the order of 1 μN, more than four orders of magnitude stronger than other actuation forces such as optical tweezers and dielectrophoresis, among others.

The equilibrium contact angle θ_e is determined by the

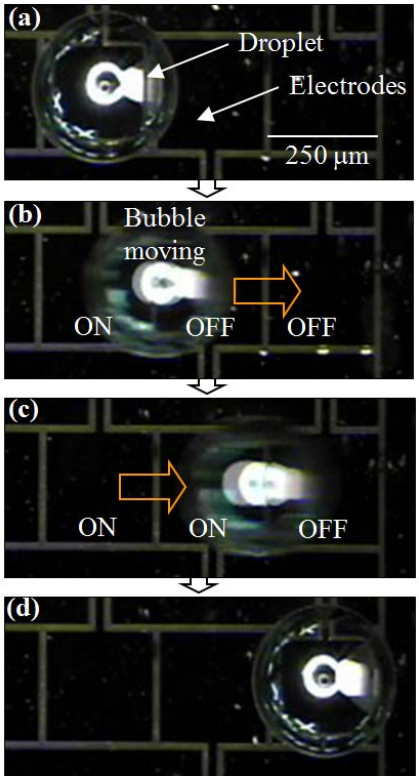

Fig. 6 Sequential pictures of air bubble transportation. Reprinted with permission[19]

interfacial tensions among the solid, liquid, and bubble phases. It is important for the contact angle modulation to be maximized by electrowetting actuation. There is an additional condition that is required to initiate the bubble motion: the contact angle hysteresis should be as small as possible. It is worth noting that the driving force linearly scales with the bubble size R according to Eq. (2), thus dominating other forces that scale in the second or higher order with the characteristic length.

Air bubble transportation is realized on addressable EWOD electrodes, as shown in Fig. 6. An air bubble (~300 μm dia.) initially sits on the left square EWOD electrode (250 × 250 μm^2), as shown in Fig. 6(a). When the left electrode is turned on while the center and right electrodes are turned off, the bubble moves to the center electrode, whose surface is hydrophobic, as shown in Fig. 6(b). To transport the bubble one step further to the right, the left and center electrodes are turned on while the right electrode is off, as shown in Fig. 6(c). The bubble then moves immediately to the adjacent right electrode again. When the EWOD electrode is activated, the initially hydrophobic surface of the electrode becomes hydrophilic, which results in the bubble being pushed to the hydrophobic surface, which is opposite to the water droplet configuration.

3. Fundamental Bubble Manipulations

Digital microfluidics based on the manipulation of discrete droplets/bubbles is a new approach to lab-on-a-chip systems, which differs from continuous microfluidics, which deals with continuous

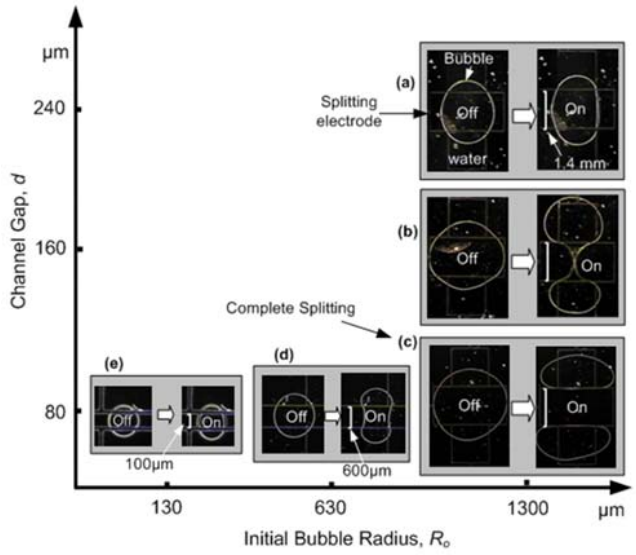

Fig. 7 Experimental verification of the bubble splitting criterion. In each case images are taken before (shown left) and after (shown right) activating the splitting electrode: (a)-(c) the effect of the channel gap $\boldsymbol{d}$ with a fixed $\boldsymbol{R_o}$ (~1300 μm). As $\boldsymbol{d}$ decreases, the bubble is further pinched in the middle and finally split into two (c); and (c)-(e) the effect of the bubble size in the condition that the ratio of the splitting electrode width and the bubble size $\boldsymbol{w/R_o}$ is about equal in all the three cases. The smaller the bubble, the more difficult it is to reach pinched shapes in the middle. Bubble volumes in (a)-(e) are 1.00, 0.87, 0.45, 0.10 and 0.004 μL, respectively. The same voltage of 90 V_{DC} is applied in all the five cases. Reprinted with permission[47]

liquid flow in microfabricated channels. Digital microfluidic systems do not require any pumps or valves, and discrete droplets/bubbles can be independently manipulated on a two-dimensional surface using electrical signal controls.[7,19] In bubble-based digital microfluidics, there are four fundamental operations: the creation, transportation, splitting, and merging of bubbles. Zhao el al.[47,49] was the first to demonstrate the fundamental manipulation of bubbles using EWOD actuation.

Figure 7 shows the dynamics of bubble splitting. Optimal splitting conditions were statically analyzed along with their experimental confirmation. It was found that a smaller channel gap, larger bubble size, wider splitting electrode, and/or larger changes in the contact angle by EWOD actuation provide the conditions favorable to successful bubble splitting. This trend is consistent with the case of droplet splitting.

In the development of bubble-based digital microfluidics, the creation and elimination of on-chip microbubbles at desired times and in the desired positions are also indispensible fundamental operations. Chung et al.[65] introduced an electrochemical method of creating on-chip microbubbles on demand. When voltages are applied between the anode and cathode electrodes patterned on the bottom plate immerged in DI water, as shown in Fig. 8, a mixed hydrogen-oxygen bubble with a diameter size ranging from several microns to several hundred microns is electrolytically created on-chip.[65,66] Figure 8(g) shows the results for the created bubble

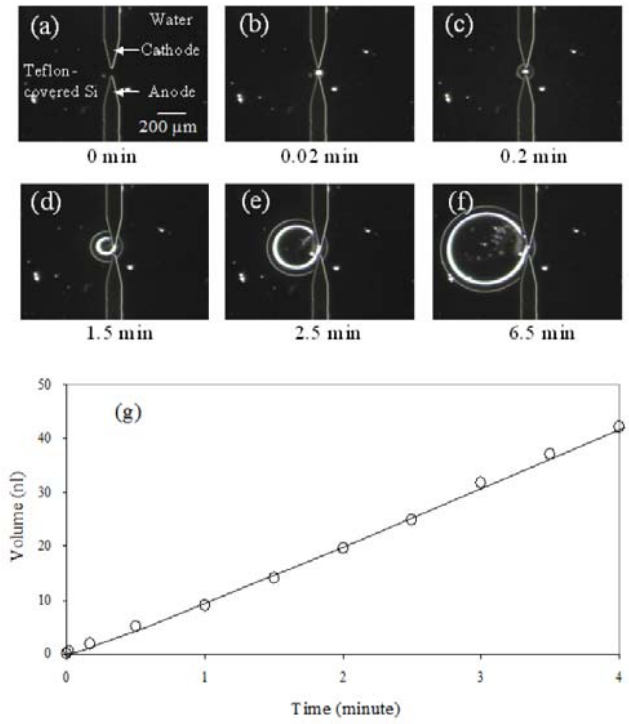

Fig. 8 Creation of hydrogen-oxygen mixture bubble. (a-f) The cathode and anode are placed on the top plate in close proximity with a separation distance of 40 μm. When a voltage (6.2 V) is applied between the cathode and anode, a hydrogen-oxygen mixture bubble is created at the tips of the electrodes and grows. (g) The bubble size is controlled by time under the constant voltage applied, ranging from 0 to 700 μm in top view diameter (0 to 45 nl in volume). Reprinted with permission[65]

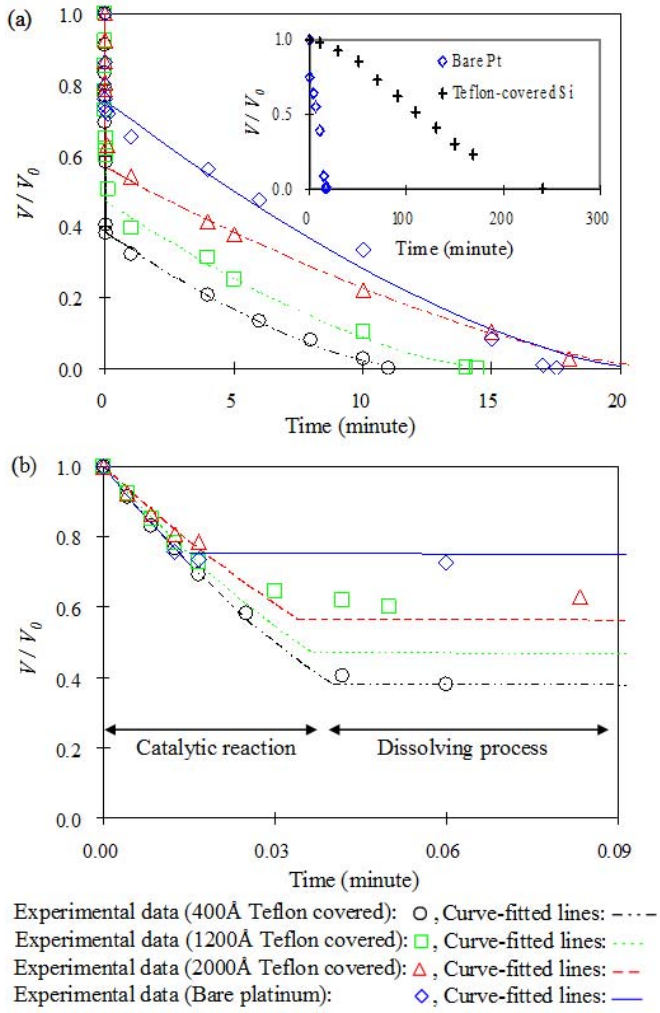

Fig. 9 Effects of the Teflon layer thickness covering the platinum electrode on bubble shrinking. The volume (V) is normalized by the initial volume (V_o = 0.6 nl) which is the same for all the cases tested. For reference, a bubble on a Teflon-covered silicon surface is also examined. The platinum electrode accelerates bubble shrinking by an order of magnitude faster than the Teflon-covered silicon surface, as shown in the inset. The thinner the Teflon layer is, the faster the bubble shrinking is. Note that the bare platinum electrode is less effective than the Teflon-covered platinum electrodes. Reprinted with permission[65]

volume with respect to the time required; the results show that a high degree of size controllability can be achieved by adjusting the time.

Without the function of on-chip bubble elimination, unwanted bubbles can cause problems such as coalescence with other bubbles, blockage of another bubble's path, or the generation of an undesired flow pattern under acoustic excitation during bubble manipulation. Zhao et al.[47] introduced a simple method for the elimination of bubbles by moving bubbles to the air-liquid interface. However, this method requires an air-water interface on a chip, which can often make chip fabrication and packaging more difficult.

Chung et al.[65] introduced another method for the elimination of on-chip bubbles. A reverse electrolytic reaction was applied with a platinum catalyst in order to accelerate the reaction rate by reducing the chemical energy barrier during the process.[61,65] A number of tests were performed to determine the relationship between the thickness of the Teflon layer on the platinum electrode and the rate of bubble elimination. As shown in Fig. 9, the bubble elimination rate increases as the thickness of the Teflon layer reduces. Interestingly, the Teflon-coated platinum electrode shows higher elimination rates than the bare platinum electrode. This is attributed to the fact that the Teflon-covered electrode (hydrophobic surface) has a larger contact area than the bare platinum electrode (hydrophilic surface).

Figure 10 shows the sequential results of the creation, transportation, and elimination of a microbubble on a small chip; the results show the complete set of fundamental bubble operations. In order to test these successive operations, testing devices that consist mainly of two parallel plates (top and bottom) were fabricated, using a standard lithographic microfabrication technology. The bottom plate contains an array of EWOD electrodes and a platinum electrode for bubble elimination, whereas the top plate has bubble generation electrodes (anode and cathode) and an EWOD ground electrode. The main fabrication process for the bottom plate consisted of three steps: the metallizing and patterning of electrodes, deposition and patterning of a dielectric layer, and deposition of a hydrophobic layer.

For the EWOD driving and bubble elimination electrodes, a

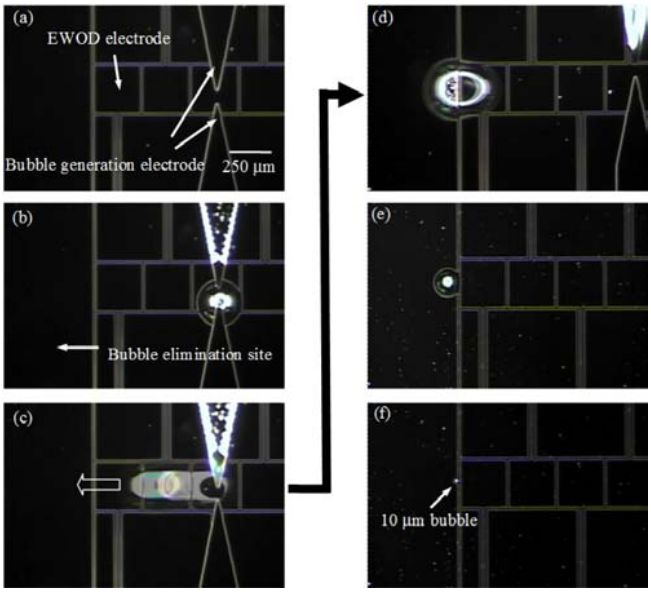

Fig. 10 Sequential images of integrated microbubble operations: generation, transportation, and elimination. (a-b) Note that the elimination site is formed by covering the platinum electrode with a 400 Å Teflon layer. A hydrogen-oxygen mixture bubble (250 μm diameter) is generated by electrolysis from the top plate and transferred to the bottom plate. (c) The bubble is transported to the left by EWOD (d) and reaches the bubble elimination site. (e) The bubble begins to shrink by the catalytic chemical reaction. (f) The bubble is shrunken down to 10 μm in diameter and is then completely removed in a few seconds. Reprinted with permission[65]

platinum layer with a thickness of 1500 Å and a chromium adhesion layer with a thickness of 100 Å were sputter-deposited onto a glass wafer and then patterned by wet etching. For the EWOD dielectric layer, a 3 μm-thick photoresist layer was spin-coated onto the entire top surface of the bottom plate. To ensure contact between the elimination electrode and the bubbles, a rectangular window (500 × 1160 μm^2) was created in the photoresist layer by a developing process. Finally, the bottom plate was coated with a hydrophobic Teflon layer.

The top glass plate fabrication consisted of metallizing and patterning of the EWOD ground and anode/cathode electrodes. A platinum layer with a thickness of 1500 Å and a chromium adhesion layer with a thickness of 100 Å were sputter-deposited onto a glass wafer and then patterned by wet etching. For integration of the top and bottom plates, a large water drop was placed on the bottom plate; then, the top plate was gently pressed against the walls that were placed on the bottom plate. Multiple layers of double-sided tape (each about 100 μm thick) were used for the walls, both to confine the water in place and to serve as spacers. For more details on the EWOD chip fabrication, refer to another article.[19]

The bubble (250 μm dia.) is created on-chip on the top plates and then transported to the left on the elimination site by EWOD actuation. The bubble on the elimination site, in which the platinum electrode is covered with a thin Teflon layer, begins to shrink and is completely eliminated within an hour. It should be noted that the hydrophobic Teflon layer on the elimination site provides two important advantages: (1) the bubble elimination time is shortened compared to the case in which a bare platinum layer is used, and (2) it allows bubbles to move on the elimination site using EWOD. Without this layer, EWOD would not be strong enough to move the bubble onto the elimination site because of the hydrophilicity of the bare platinum surface.

4. Applications of Bubble-Based Microfluidics

4.1 Microstreaming Flow/Radiation Force

EWOD provides bubbles with lateral mobility. This functionality of bubbles can be enhanced by integrating EWOD with additional modes of actuation. Because bubbles contain compressible gases, they are susceptible to disturbance by external pressures. When a gaseous bubble is acoustically excited near the bubble's resonant frequency, the bubble oscillates, generating strong vertical flows around it. This phenomenon is called cavitational microstreaming.[67,68] Marmottant el al.[69,70] analytically derived the streaming function of a cavitational streaming flow for an axisymmetric oscillating bubble sitting on a wall as follows:

$$\psi = -3\varepsilon^2 a^3 \omega \sin(\Delta\phi)\frac{a}{r}\cos^2\theta\sin^2\theta + O(\varepsilon^2 r^{-2}) \qquad (3)$$

Here, ε is the amplitude of bubble oscillation normalized by the radius of the bubble a, ω is the angular frequency of the applied acoustic wave, r is the distance from the bubble center, θ is the angle coordinate with respect to the axis of translation, and $\Delta\phi$ is the phase shift between volume and translational oscillations. Figure 11 shows that the theoretical result is well matched with the experimental result, which is based on a microbubble (~15 μm dia.).

Ko et al.[71] recently found that a bubble under forced alternating current electrowetting-on-dielectric (AC-EWOD) actuation at low frequencies also behaves similarly to an acoustically oscillating bubble. Figure 12 shows strong streaming flows (called synthetic jets) from a bubble actuated by AC-EWOD in an aqueous electrolyte solution. The speed of the synthetic jet is proportional to the oscillation amplitude of the bubble, and the jet speed reaches a maximum at the natural oscillation frequencies. It should be noted that the bubble oscillation amplitudes in Fig. 12 are measured from high-speed images, but they can also be analytically predicted by the superposition of Legendre polynomials. These streaming flows can be utilized in the control of flow patterns and thus in the steering of objects immersed in streaming flows.[70]

Bubble oscillation generates not only a microstreaming flow around it but also an attraction/repulsion force, the so-called radiation force (or Bjerknes force), which depends on the size and density of the medium and object.[67,72] An oscillating bubble emits spherical acoustic waves and generates nodes and antinodes in the sound pressure field around the bubble. Miller[73] reported that particle attraction occurs when a gas trapped in a microspore is ultrasonically excited. The capturing of microparticles and various objects using oscillating bubbles was intensively studied by Chung et al..[39,74-76] The effects of the frequency and amplitude of acoustic

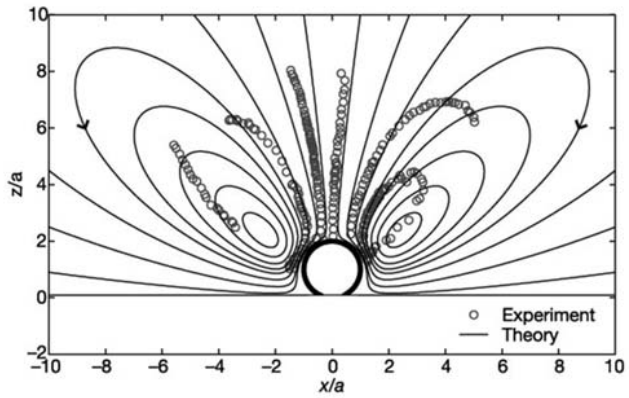

Fig. 11 Streamlines of the computed flow field (for z > 0), superimposed on a number of measured vesicle trajectories, scaled properly. Deviations between experiment and theory show the influence of weak streaming around the vesicles. Reprinted with permission[69]

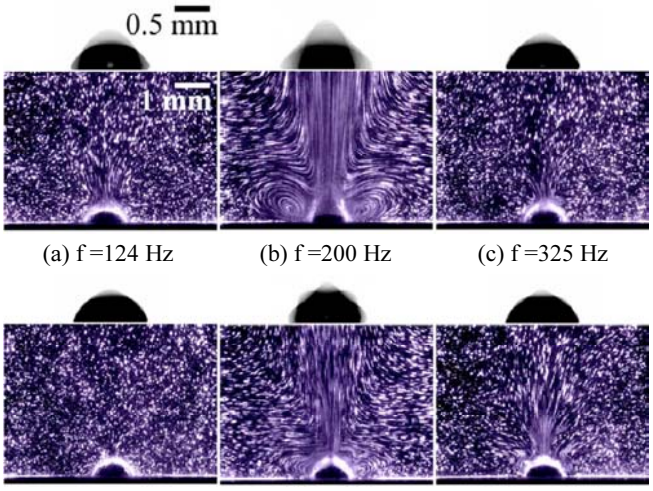

Fig. 12 Streamlines and oscillation patterns for oscillating bubbles for different frequencies. Δ=1 μl and V_{rms}=80 V. Reprinted with permission[71]

excitation and AC-EWOD actuation on the capturing of microparticles are quantified with the bubble oscillation amplitude using high-speed imaging.[75] Figure 13 shows the effects of frequency on capturing by AC-EWOD actuation. When a bubble (~400 μm dia.) is oscillated by AC-EWOD of 100 Hz, neighboring glass beads (80 μm) are captured on the bubble (Fig. 13(a-1,2)). However, when the frequency is shifted to 1 kHz, the degree of capturing is not significant (Fig. 13(a-3)) because of the small oscillation amplitude. Similar results were obtained with a 1 mm bubble (Fig. 13(b-1,2)). Figure 13(c) shows that an oscillating bubble moves randomly on the surface because of a large oscillation amplitude, and captures and carries a fish egg without losing it during its lateral motion.

4.2 Manipulation of Bio/Micro-object

By utilizing the capturing phenomenon described above, a method of manipulating micro-objects via a mobile oscillating

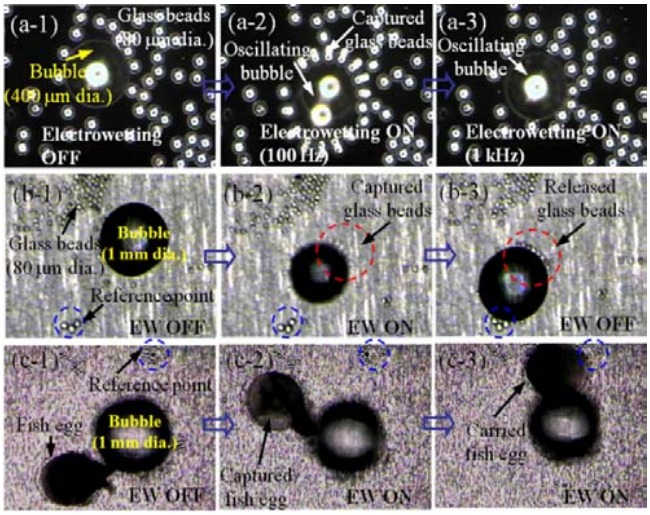

Fig. 13 Capturing and carrying of glass beads and a fish egg using oscillating bubbles: (a-1) Initial state (bubble size ~400 μm), (a-2) Strong capturing of glass beads (100 Hz AC-EWOD), (a-3) Weak capturing (1 kHz AC-EWOD); (b) Similar to case (a) except bubble size (~1 mm dia); (c-1) Initial state, (c-2) A fish egg (~ 1 mm) is captured on the oscillating bubble (100 Hz AC-EWOD), (c-3) When the bubble moves randomly due to large oscillation, the fish egg is carried by the bubble. Reprinted with permission[75] (© 2009 IEEE)

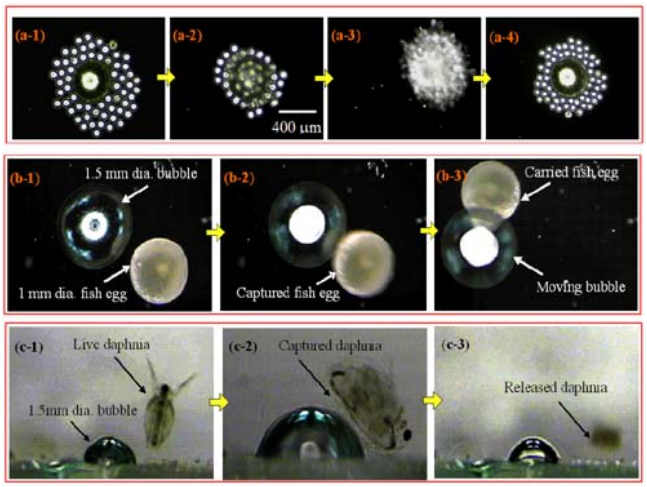

Fig. 14 Capturing of various objects using oscillating bubbles: (a-1) Initial state, (a-2) More than 60 glass particles (80 μm dia) are captured in orbit by the oscillating bubble when the piezo-actuator is turned on (200 V), (a-3) The oscillating bubble, at its natural frequency of 15 kHz, erratically and randomly moves on the surface carrying the captured particles, (a-4) Turning off acoustic excitation releases the captured particles; (b-1) Initial state, (b-2) A fish egg (~1 mm in diameter) is attracted to the oscillating bubble which is acoustically excited at 4.5 kHz, (b-3) The captured fish egg is carried by the oscillating bubble in erratic motion on the surface; (c-1 and -2) A live water flea (Daphnia) is captured by an oscillating bubble acoustically excited at 4.5 kHz, (c-3) The water flea can escape only when the bubble oscillation is turned off. Note that the applied voltage to the piezo-actuator in (b) and (c) is 400 V. Reprinted with permission[39]

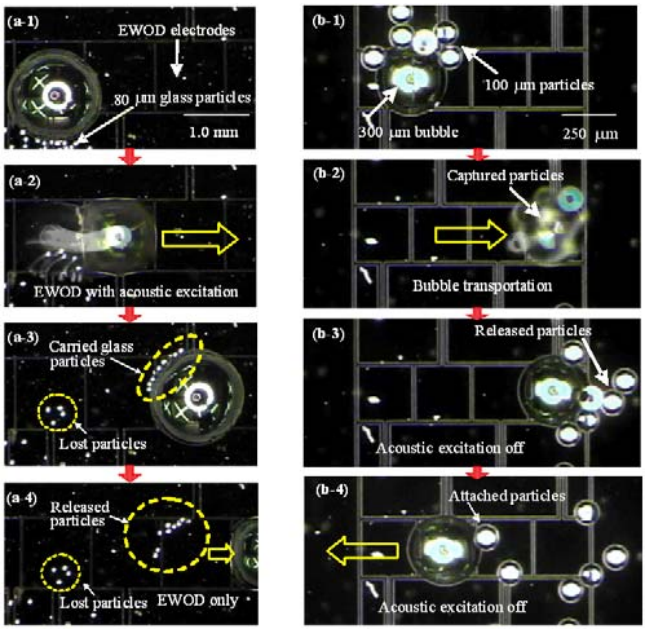

Fig. 15 Sequential pictures showing that an oscillating bubble captures, carries, and releases neighboring glass particles: (a) Bubble size 1.5 mm with glass beads: (a-1) Initial state, (a-2) With acoustic excitation (at 4.2 kHz, 300 V) on and EWOD on, the oscillating bubble captures and carries glass beads (80 mm), (a-3) The carried particles are released with acoustic excitation off, (a-4) The carried particles are completely detached from the bubble when acoustic excitation is turned off, and the bubble continues to move to the right by EWOD only (Note that the captured and carried particles are circled by yellow broken lines); (b) Bubble size 300 μm with polystyrene particles (contact angle ~66°): (b-1) Initial state; (b-2) A 300-μm diameter oscillating bubble captures and carries 100-μm polystyrene particles to the right under acoustic excitation (at 20 kHz, 150 V) and with EWOD on, (b-3) Acoustic excitation off, (b-4) Most of the particles, except one, are completely detached from the bubble when the bubble is moved by EWOD to the left with acoustic excitation off. The attachment of the particle is due to hydrophobicity of the particle. Reprinted with permission[39]

bubble was developed by Chung et al..[39] A microbubble object manipulation system (so-called microbubble tweezers) consists of a top and bottom plate with a piezo-actuator attached beneath the bottom plate. In this system, a bubble can be electrochemically created on-chip by electrolysis and then transported on any two-dimensional surface by EWOD actuation, as shown in Fig. 10. When a bubble is excited by the piezo-actuator near its resonant frequency, the oscillating bubble captures micron- and millimeter-sized particles by means of the radiation attraction force generated by the oscillating bubble. The captured particles can then be carried by the oscillating bubble via EWOD actuation. When the particles arrive at the desired location, they can be released from the bubble by turning off the piezo-actuator excitation. Furthermore, the bubble can be eliminated on-chip by the reverse electrochemical reaction. A variety of objects, including microbeads, a fish egg, and a live water flea were successfully captured, as shown in Fig. 14. The effects of the frequency and amplitude of acoustic excitation on the capturing of objects were quantified using high-speed bubble imaging.

In order to demonstrate a series of integrated operations such as the capture, carry, and release of particles in a controllable manner, an EWOD-driving mechanism was incorporated with the acoustic excitation. Two bubbles of different sizes (1.5 mm and 300 μm in diameter) were examined, as shown in Fig. 15. When the piezo-actuator attached on the bottom of the substrate was turned on, the bubble (1.5 mm dia.) oscillated and captured near 80 μm glass particles. The bubble was then transported to the right by sequentially activating the EWOD electrodes, as shown in Fig. 15(a-2). While the bubble was being transported, the captured particles were also carried with the bubble. After the bubble crossed two electrodes, the piezo-actuator was turned off. The trapped particles were released from the bubble surface and remained on the bubble rim, as shown in Fig. 15(a-3). As the bubble was transported further to the right with the acoustic excitation turned off, the particles separated from the bubble completely.

To improve a bubble's particle-carrying efficiency, the electrode actuation scheme was modified by increasing the number of inactivated EWOD electrodes from one to two during bubble transportation. This scheme provides not only a larger surface on which the bubble can be placed but also less deformation of the bubble. After this improvement of the EWOD electrode actuation scheme, multiple experiments were performed and the results showed that the carrying efficiency of oscillating bubbles for glass and polystyrene particles was over 95 % with minimal particle loss.

Similar operations using a smaller bubble (300 μm in diameter) were also examined using 100 μm polystyrene particles. When the bubble moved to the left after the operations of capturing and carrying the polystyrene particles, one particle still remained in contact with the bubble surface without separating from it completely because of the hydrophobicity of the polystyrene particles, as shown in Fig. 15(b-4). It should be noted that this problem was not observed with the glass particles and can be eliminated by adding a small amount of surfactant to reduce the adhesion between the bubble and the polystyrene particles.

4.3 Electrolysis-Bubble-Actuated Micropump

Microbubbles generated by electrolysis have been used in various microfluidic applications such as a valve,[77] a pump[78] and an actuator.[66] Recently, Yang et al.[79] introduced an electrolysis-bubble-actuated micropump that uses EWOD actuation to form an air valve in microchannels. Figure 16 shows sequential images of microfluid being pumped. When the 1st and 2nd EWOD electrodes were turned on, the surface property of the electrodes changed from hydrophobic to hydrophilic. As a result, the microchannel that contains the EWOD electrodes was filled with microfluid. When the 1st EWOD electrode was turned off, an air bubble was simultaneously trapped in the EWOD electrode, and the microfluid inside the microchannel was then transported to the right by sequential electrolysis-bubble actuations. This pump can eliminate the drawbacks of current mechanical pumps, such as the

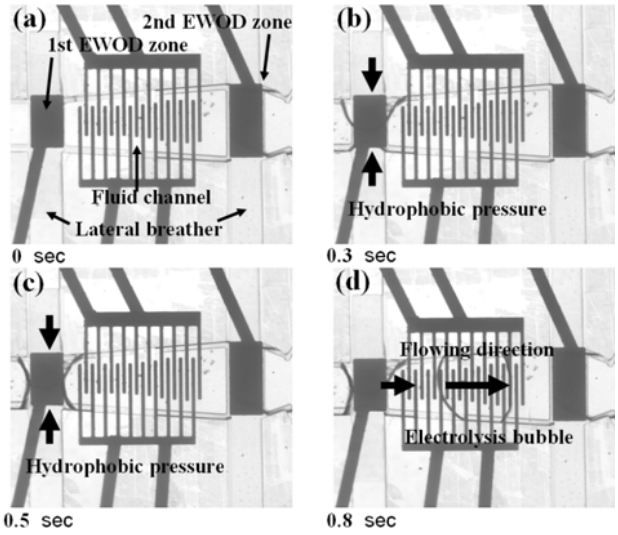

Fig. 16 Time-sequential recorded pictures. (a) The voltage difference is applied at first and second EWOD zones. (b) The voltage at first EWOD zone is turned off. (c) An air valve is formed. (d) Microfluid is pumped without back flow. Reprinted with permission[79] (© 2009 IEEE)

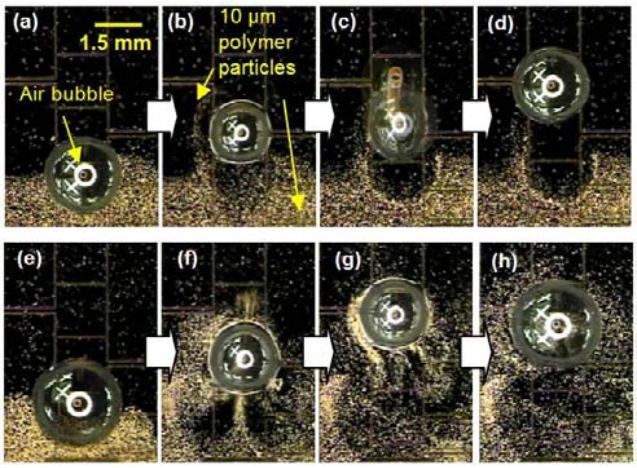

Fig. 17 Comparison of mixing for four cases. Top and bottom images show the initial states and the final states after 2 minutes actuation, respectively. (a) mixing by diffusion only (case 1), (b) mixing by an EWOD-actuated bubble without acoustic excitation (case 2). (c) mixing by an oscillating bubble without EWOD transportation (case 3) (d) mixing by an oscillating mobile bubble actuated EWOD and acoustic wave (case 4). In the order from case 1 to case 4, the mixing performance becomes better. Reprinted with permission[81]

diminishing of performance and reliability caused by long-term operation fatigue, because EWOD actuation requires no mechanical moving parts.

4.4 Oscillating Mobile Bubble Mixer

A cavitational microstreaming flow from an oscillating bubble is used to agitate the surrounding fluid in a small chamber in tandem with EWOD actuation to produce bubble mobility. Liu et al.[80] was the first to utilize oscillating bubbles to agitate the surrounding fluid to enhance the mixing process. However, the oscillating bubbles were fixed in predetermined places and had no mobility; therefore, a significant time was still required for the flow agitation to propagate from the bubble to the end of the mixing chamber.

Chung et al.[81] developed a highly efficient method of fluid mixing that uses an acoustically oscillating mobile bubble. Four different combinations of two kinds of actuation (acoustic actuation and EWOD actuation) were examined in terms of mixing enhancement, as shown in Fig. 17. A series of experiments showed that the stirring of fluid by the oscillation of mobile bubbles significantly reduces the time it takes for the stirred fluid to reach the end of mixing chamber, thus augmenting the mixing efficiency.

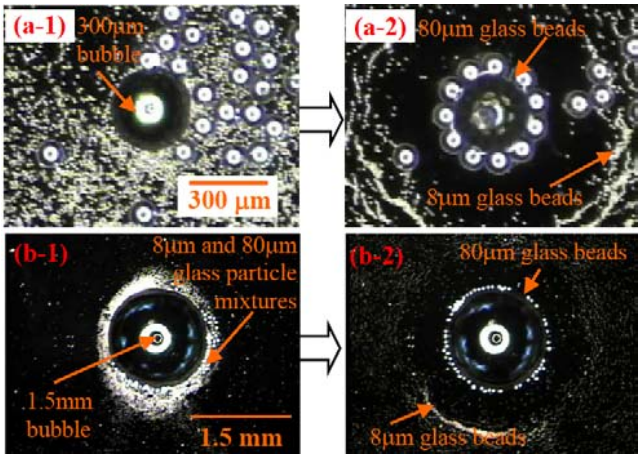

Fig. 18 Sequential pictures showing that acoustically excited oscillating bubbles can separate particles of two different sizes. (a) With a 300 μm bubble and mixtures of 8 μm and 80 μm glass particles: (a-1) Initial state; (a-2) After acoustic excitation, most of the 80 μm particles are collected near the bubble whereas the 8 μm particles are repelled away; (b) With a 1.5 mm bubble and mixtures of 8 μm and 80 μm glass particles: (b-1) Initial state; (b-2) After acoustic excitation, the 80 μm particles are collected around the bubble whereas the 8 μm particles are repelled away. Reprinted with permission[82]

4.5 Separation and Collection of Microparticles Using Oscillating Bubbles

Ryu et al.[82] demonstrated a novel method that uses oscillating microbubbles to separate microparticles by size and to collect them. Figure 18 shows the separation and collection of particles of two different sizes (80 μm and 10 μm in diameter). When the bubbles oscillate, the neighboring particles are influenced by both the acoustic radiation (Bjerknes) force and the microstreaming flow. However, the larger particles experience stronger radiation force than the smaller ones. For this reason, the larger particles are attracted to the oscillating bubbles, whereas the smaller ones follow the streaming flow pattern and thus scatter randomly. As shown in Fig. 18(a-2) and (b-2), after acoustic excitation is applied to the bubbles for several seconds, the 80 μm glass particles collect at the rims of the bubbles, whereas the 8 μm glass particles are scattered away from the oscillating bubbles. It should be noted that the

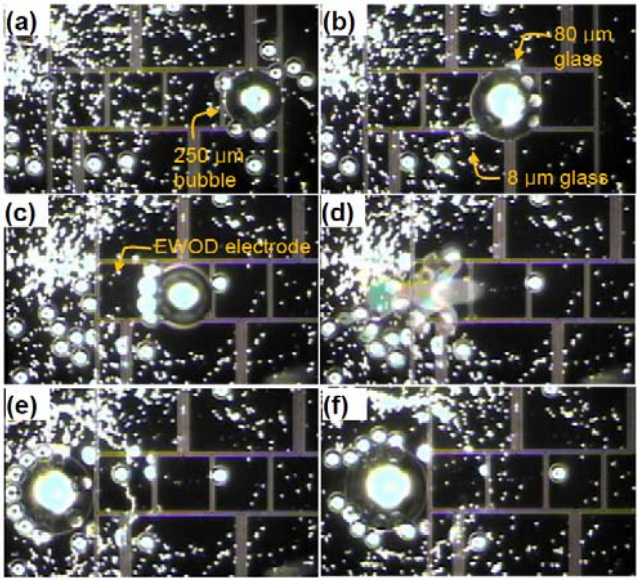

Fig. 19 A bubble of 250 μm diameter is transported to the left by EWOD and oscillated by acoustic excitation at 20 kHz (a) initial condition (b-d) The oscillating bubble traps and carry 80 μm particles, not 8 μm particles while in lateral motion. (e-f) releasing 80 μm particles. Reprinted with permission[82]

particles were initially mixed and deposited around the bubbles.

Figure 19 shows the integration of this separation achieved with EWOD. A mobile oscillating bubble can selectively trap and separate particles. An acoustically oscillating bubble is transported step-by-step to the left by EWOD actuation, simultaneously trapping and carrying 80 μm particles; however, the 8 μm particles are repelled from the bubble and are scattered everywhere. As a result, most of the 80 μm particles are collected on the left side, as shown in Fig. 19(e-f).

4.6 Propulsion of Objects Floating on Water

EWOD can be applied to the propulsion of mini/micro-objects. Chung et al.[83] developed mini/micro-boats or robots, which have no mechanical moving parts and can swim on a water-free surface like a water strider.[84-87] A centimeter-sized mini-boat was fabricated from a thin plastic foil with outer surfaces that were covered with electrodes for EWOD actuation. By applying a voltage to the electrodes, the boat is propelled, as shown in Fig. 20.

For linear transportation, two EWOD electrodes are attached to both the front and rear sides of the boat. When voltages are applied to the rear electrode, as shown by the red broken circle in Fig. 20(a), the boat moves forward. Similarly, the activation of the front electrode generates a reverse motion (not shown), which confirms that EWOD actuation generates a propulsive force. For a rotational motion, two electrodes are used: one attached to a side face and the other to the face on the opposite side. These electrodes are diagonally aligned to each other, as shown by the red broken circle in Fig. 20(b). When voltages are applied to both electrodes, the boat rotates in a clockwise direction. By combining linear and rotational motions, a curvilinear motion was also demonstrated, as shown in Fig. 20(c).

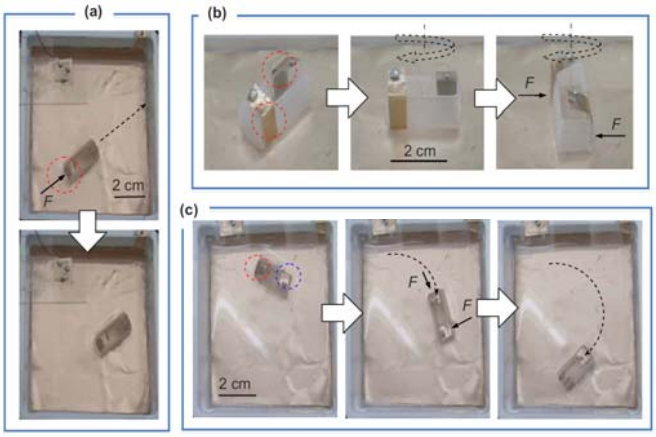

Fig. 20 Sequential snapshots of mini/micro-boat propulsion. The broken circles denote activated electrodes, the broken arrows indicate the boat path, and the solid arrows show the generated propulsion forces. (a) Linear propulsion. When a voltage of 160 V (1 kHz) is applied to the electrode in the boat stern, the forward moving speed is measured at 4 mm/ s. (b) Rotation. The boat is rotated at ~20 rpm when 140 V (1 kHz) is applied to two electrodes, which are attached to the side faces in a diagonal arrangement. (c) Curvilinear propulsion. The boat is propelled along a curved path when 160 V (1 kHz) is applied to the electrode on the side face in the boat bow and the electrode in the boat stern at the same time, demonstrating steering capability. Reprinted with permission[83]

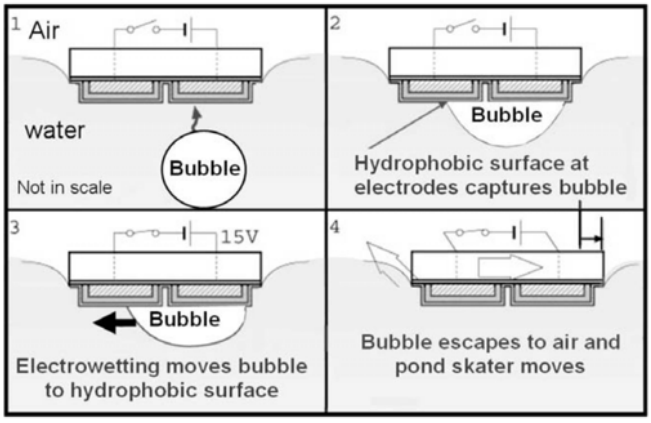

Fig. 21 Illustration of the propulsion mechanism for the EWOD pond skater. (1) Movement of an air bubble towards an electrode. (2) Bubble capture. (3) Fifteen volts applied between the electrodes changes the right electrode surface to hydrophilic, thus moving the bubble to the left. (4) The bubble escapes from the left edge, causing a counter-movement of the pond skater chip. The distance moved is identified. Reprinted with permission[89]

The maximum measured linear propulsion speed and rotation rate were 5 mm/s and 20 rpm, respectively. It is observed that propulsion takes place only when AC-EWOD is applied, not DC-EWOD. The mechanism of propulsion is that AC-EWOD produces oscillations in the water on the surface of the EWOD electrodes and generates streaming flows that are outgoing relative to the EWOD electrode surface. In turn, this outgoing streaming flow pushes the EWOD electrode. The method for this novel propulsion and

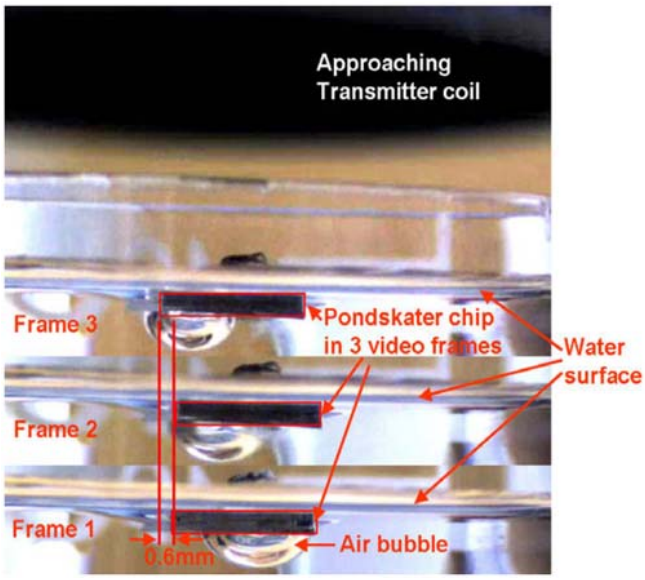

Fig. 22 Three consecutive frames (1-3) showing the pond skater movement during the air bubble displacement driven by wireless power transmission. Reprinted with permission[89]

rotation mechanism is simple yet efficient; this method can possibly be used to propel and maneuver mini/micro-water-floating boats and robots that can be used for water/air quality monitoring systems or security surveillance systems for specific purposes in other industry areas.[83,88]

Mita et al.[89] developed a silicon-based swimming robot or pond skating device that floats on liquid surfaces through the use of surface tension and is propelled by EWOD. Figure 21 shows the schematics of the propulsion mechanism involved. The bubble moves from the front to the back of the boat by EWOD actuation. In reaction, the boat moves in the direction opposite to that of the bubble. To develop this concept, a small device (6 × 9 mm) was fabricated on a piece of silicon that was coated with a high permittivity material (Ta_2O_5) as a dielectric layer for low-voltage EWOD actuation, which was low enough to enable RF power transmission to propel the object floating on water, as shown in Fig 22. While they were able to demonstrate propulsion for a short distance using a single bubble, this method requires the continuous creation of bubbles in order to generate continuous movement.

4.7 Propulsion of Underwater Objects

The above propulsion methods work for objects floating on water, not underwater objects. The development of the micropropulsion of microrobots for underwater objects has a great potential for applications such as drug delivery and microsurgery.[90-95] Chung et al.[96] were the first to propose a novel underwater propulsion technique that uses acoustically excited oscillating bubbles and offered experimental proof of its functionality. Later, Ryu et al.[97] improved this technique with a similar propulsion technique that uses bubbles oscillated by AC-EWOD actuation. To prove their concept of propulsion, air bubbles (300 μm dia. or 1.5 mm dia.) were positioned on the surface of various underwater objects ranging in size from a few hundred microns to centimeters. It should be noted that the surfaces of the underwater objects had a single EWOD electrode for the actuation of bubbles. When an AC-EWOD signal was applied between the surfaces of the objects and the water medium, the bubbles oscillated at the frequency of the applied signal and generated steady streaming flows around the bubbles. The streaming flows in turn generated forces reactive to the objects, resulting in the propulsion of the objects. For a rotational motion, a pair of EWOD electrodes was installed on a centimeter-sized object. When an electrowetting signal was transferred by wire or wirelessly to the electrodes, the object was rotated. These results experimentally prove that oscillating bubbles can propel underwater objects. Unlike conventional propulsion, this technique does not require any solid moving parts and can thus provide a simple and efficient propulsion mechanism for microrobots that can swim inside the human body.

5. Summary

Electrowetting-on-dielectric (EWOD) is currently enjoying a renaissance of interest and is making great contributions in many areas from microfluidics to optics. Although most of the related research work has been focused on droplet operations using EWOD, EWOD can also be applied to bubbles, which could spawn a variety of potential applications. This paper has therefore reviewed the theoretical background and demonstrated applications of EWOD with bubbles. The concept of bubble-based EWOD was discussed in terms of the fundamental bubble operations, in which an on-chip bubble can be created, transported, split, and eliminated. These fundamental operations can then be extended to more advanced operations that involve the mixing and pumping of fluids and particles. Unlike droplets, bubbles can be easily oscillated by external excitation because gaseous bubbles are quite susceptible to external disturbances. By integrating the fundamental operations of EWOD with acoustic excitation, new functionalities of bubbles have been developed for the capture and separation of particles and the propulsion of objects. In these advanced functions, microstreaming flows and acoustic radiation forces are the key factors that animate the physical mechanisms. The capturing/separating function may provide new solutions to the efficient tweezing of micro/bio-objects, and the propulsion function may allow us to develop a remotely controlled bio/micro-robot that can swim inside the human body. In addition to bubble oscillation, it is expected that other modes of bubble actuation will be integrated with EWOD operations, which may open the door to even more interesting and useful applications in the future.

ACKNOWLEDGEMENT

Authors thank Kyung Ho Lee, Jung Min Won, Jeong Hyun Lee, Jung Byung Chae, Jun O Kwon, Tae Gon Kim and Ji Sun Yang for literature survey. This work was supported by 2010 Research Fund of Myongji University in Korea.

REFERENCES

1. Whitesides, G. M., "The origins and the future of microfluidics," Nature, Vol. 442, No. 7101, pp. 368-373, 2006.
2. Fair, R. B., "Digital microfluidics: is a true lab-on-a-chip possible?" Microfluidics and Nanofluidics, Vol. 3, No. 3, pp. 245-281, 2007.
3. Cho, S. K., Moon, H. J. and Kim, C. J., "Creating, transporting, cutting, and merging liquid droplets by electrowetting-based actuation for digital microfluidic circuits," Journal of Microelectromechanical Systems, Vol. 12, No. 1, pp. 70-80, 2003.
4. Haeberle, S. and Zengerle, R., "Microfluidic platforms for lab-on-a-chip applications," Lab on a Chip, Vol. 7, No. 9, pp. 1094-1110, 2007.
5. Hong, J. W. and Quake, S. R., "Integrated nanoliter systems," Nature biotechnology, Vol. 21, No. 10, pp. 1179-1183, 2003.
6. Jakeway, S. C., Mello, A. J. d. and Russell, E. L., "Miniaturized total analysis systems for biological analysis," Fresenius Journal of Analytical Chemistry, Vol. 366, No. 6-7, pp. 525-539, 2000.
7. Cho, S. K. and Moon, H., "Electrowetting on dielectric (EWOD): New tool for bio/micro fluids handling," The BioChip Journal, Vol. 2, No. 2, pp. 79-96, 2008.
8. Beebe, D. J., Mensing, G. A. and Walker, G. M., "Physics and applications of microfluidics in biology," Annu. Rev. Biomed. Eng., Vol. 4, No. 1, pp. 261-286, 2002.
9. Purcell, E. M., "Life at low Reynolds number," American Journal of Physics, Vol. 45, No. 1, pp. 3-11, 1977.
10. Burgreen, D. and Nakache, F. R., "Electrokinetic Flow in Ultrafine Capillary Slits," Journal of Physical Chemistry, Vol. 68, No. 5, pp. 1084-1091, 1963.
11. Holmes, D., Green, N. G. and Morgan, H., "Microdevices for Dielectrophoretic Flow-Through Cell Separation," Engineering in Medicine and Biology Magazine, Vol. 22, No. 6, pp. 85-90, 2003.
12. Klingner, A., Buehrle, J. and Mugele, F., "Capillary bridges in electric fields," Langmuir, Vol. 20, No. 16, pp. 6770-6777, 2004.
13. Morgan, H. and Green, N. G., "AC Electrokinetics: colloids and nanoparticles," Research Studies Press, 2003.
14. Patankar, N. A. and Hu, H. H., "Numerical Simulation of Electroosmotic Flow," Analytical Chemistry, Vol. 70, No. 9, pp. 1870-1881, 1998.
15. Prins, M. W. J., Welters, W. J. J. and Weekamp, J. W., "Fluid control in multichannel structures by electrocapillary pressure," Science, Vol. 291, No. 5502, pp. 277-280, 2001.
16. Rice, C. L. and Whitehead, R., "Electrokinetic Flow in a Narrow Cylindrical Capillary," Journal of Physical Chemistry, Vol. 69, No. 11, pp. 4017-4024, 1965.
17. Welters, W. J. J. and Fokkink, L. G. J., "Fast electrically switchable capillary effects," Langmuir, Vol. 14, No. 7, pp. 1535-1538, 1998.
18. Mugele, F. and Baret, J. C., "Electrowetting: From basics to applications," Journal of Physics-Condensed Matter, Vol. 17, No. 28, pp. R705-R774, 2005.
19. Chung, S. K., Zhao, Y. and Cho, S. K., "Electrowetting-On-Dielectric (EWOD) Microfluidic Devices," Lab on a Chip (LOC) Technologies and Applications, Edited by Keith E. Herold and Avi Rasooly, Horizon Scientific Press and Caister Academic Press, pp. 211-229, 2009.
20. Kang, K. H., "How electrostatic fields change contact angle in electrowetting," Langmuir, Vol. 18, No. 26, pp. 10318-10322, 2002.
21. Zeng, J. and Korsmeyer, T., "Principles of droplet electrohydrodynamics for lab-on-a-chip," Lab on a Chip, Vol. 4, No. 4, pp. 265-277, 2004.
22. Collet, P., De Coninck, J., Dunlop, F. and Regnard, A., "Dynamics of the contact line: Contact angle hysteresis," Physical Review Letter, Vol. 79, No. 19, pp. 3704-3707, 1997.
23. Huh, D., Tkaczyk, A. H., Bahng, J. H., Chang, Y., Wei, H. H., Grotberg, J. B., Kim, C. J., Kurabayashi, K. and Takayama, S., "Reversible switching of high speed air liquid two phase flows using electrowetting assisted flow pattern change," Journal of the American Chemical Society, Vol. 125, No. 48, pp. 14678-14679, 2003.
24. Mugele, F., Klingner, A., Buehrle, J., Steinhauser, D. and Herminghaus, S., "Electrowetting: a convenient way to switchable wettability patterns," Journal of physics: condensed matter, Vol. 17, No. 9, pp. S559-S576, 2005.
25. Berge, B. and Peseux, J., "Variable focal lens controlled by an external voltage: An application of electrowetting," The European Physical Journal E, Vol. 3, No. 2, pp. 159-163, 2000.
26. Krupenkin, T., Yang, S. and Mach, P., "Tunable liquid microlens," Applied Physics Letters, Vol. 82, No. 3, pp. 316-318, 2003.
27. Kuiper, S. and Hendriks, B. H. W., "Variable-focus liquid lens for miniature cameras," Applied Physics Letters, Vol. 85, No. 7, pp. 1128-1130, 2004.
28. Hou, L., Zhang, J., Smith, N., Yang, J. and Heikenfeld, J., "A full description of a scalable microfabrication process for arrayed electrowetting microprisms," Journal of Micromechanics and Microengineering, Vol. 20, No. 1, Paper No. 015044, 2010.

29. Smith, N. R., Abeysinghe, D. C., Haus, J. W. and Heikenfeld, J., "Agile wide-angle beam steering with electrowetting microprisms," Optics Express, Vol. 14, No. 14, pp. 6557-6563, 2006.

30. Beni, G. and Tenan, M. A., "Dynamics of electrowetting displays," Journal of applied physics, Vol. 52, No. 10, pp. 6011-6015, 1981.

31. Hayes, R. A. and Feenstra, B. J., "Video-speed electronic paper based on electrowetting," Nature, Vol. 425, No. 6956, pp. 383-385, 2003.

32. Roques-carmes, T., Hayes, R. A., Feenstra, B. J. and Schlangen, L. J. M., "Liquid behavior inside a reflective display pixel based on electrowetting," Journal of applied physics, Vol. 95, No. 8, pp. 4389-4396, 2004.

33. Acharya, B. R., Krupenkin, T., Ramachandran, S., Wang, Z., Huang, C. C. and Rogers, J. A., "Tunable optical fiber devices based on broadband long period gratings and pumped microfluidics," Applied Physics Letters, Vol. 83, No. 24, pp. 4912-4914, 2003.

34. Cheng, J.-Y. and Hsiung, L.-C., "Electrowetting (EW)-Based Valve Combined with Hydrophilic Teflon Microfluidic Guidance in Controlling Continuous Fluid Flow," Biomedical Microdevices, Vol. 6, No. 4, pp. 341-347, 2004.

35. Chioua, P. Y., Moonb, H., Toshiyoshic, H., Kimb, C. J. and Wua, M. C., "Light actuation of liquid by optoelectrowetting," Sensors and actuators A: physical, Vol. 104, No. 3, pp. 222-228, 2003.

36. Hoshino, K., Triteyaprasert, S., Matsumoto, K. and Shimoyama, I., "Electrowetting-based pico-liter liquid actuation in a glass-tube microinjector," Sensors and actuators A: physical, Vol. 114, No. 2-3, pp. 473-477, 2004.

37. Shen, N. Y., Liu, Z., Jacquot, B. C., Minch, B. A. and Kan, E. C., "Integration of chemical sensing and electrowetting actuation on chemoreceptive neuron MOS (CvMOS) transistors," Sensors and actuators B: chemical, Vol. 102, No. 1, pp. 35-43, 2004.

38. Zhao, Y. J. and Cho, S. K., "Microparticle sampling by electrowetting-actuated droplet sweeping," Lab on a Chip, Vol. 6, No. 1, pp. 137-144, 2006.

39. Chung, S. K. and Cho, S. K., "On-chip manipulation of objects using mobile oscillating bubbles," Journal of Micromechanics and Microengineering, Vol. 18, No. 12, Paper No. 125024, 2008.

40. Srinivasan, V., Pamula, V. K. and Fair, R. B., "Droplet-based microfluidic lab-on-a-chip for glucose detection," Analytica Chimica Acta, Vol. 507, No. 1, pp. 145-150, 2004.

41. Lippmann, G., "Relations entre les ph´enom`enes ´electriques et capillaires," Ann. Chim. Phys., Vol. 5, No. 11, pp. 494-549, 1875.

42. Quilliet, C. and Berge, B., "Electrowetting: a recent outbreak," Current opinion in colloid & Interface science, Vol. 6, No. 1, pp. 34-39, 2001.

43. Quilliet, C. and Berge, B., "Investigation of effective interface potentials by electrowetting," Europhysics letters, Vol. 60, No. 1, pp. 99-105, 2002.

44. Kang, K. H., Kang, I. S. and Lee, C. M., "Electrostatic contribution to line tension in a wedge-shaped contact region," Langmuir, Vol. 19, No. 22, pp. 9334-9342, 2003.

45. Jones, T. B., "On the relationship of dielectrophoresis and electrowetting," Langmuir, Vol. 18, No. 11, pp. 4437-4443, 2002.

46. Jones, T. B., "An electromechanical interpretation of electrowetting," Journal of Micromechanics and Micro-engineering, Vol. 15, No. 6, pp. 1184-1187, 2005.

47. Zhao, Y. and Cho, S. K., "Micro Air Bubble Manipulation by Electrowetting on Dielectric: transporting, splitting, merging and eliminating of bubbles," Lab on a Chip, Vol. 7, No. 2, pp. 273-280, 2007.

48. Berry, S., Kedzierski, J. and Abedian, B., "Irreversible Electrowetting on Thin Fluoropolymer Films," Langmuir, Vol. 23, No. 24, pp. 12429-12435, 2007.

49. Zhao, Y. and Cho, S. K. "Micro bubble manipulation towards single cell handling tool," Proceedings of IEEE International Conference on Robotics and Biomimetics, pp. 269-273, 2005.

50. Janocha, B., Bauser, H., Oehr, C., Brunner, H. and Gopel, W., "Competitive Electrowetting of Polymer Surface by Water and Decane," Langmuir, Vol. 16, No. 7, pp. 3349-3354, 2000.

51. Moon, H., Cho, S. S., Garrell, R. L. and Kim, C. J., "Low voltage electrowetting on dielectric," Journal of applied physics, Vol. 92, No. 7, pp. 4080-4087, 2002.

52. Peykov, V., Quinn, A. and Ralston, J., "Electrowetting: a model for contact angle saturation," Colloid and Polymer Science, Vol. 278, No. 8, pp. 789-793, 2000.

53. Shapiro, B., Moon, H., Garrell, R. L. and Kim, C.-J., "Equilibrium behavior of sessile drops under surface tension, applied external fields, and material variations," Journal of Applied Physics, Vol. 93, No. 9, pp. 5794-5811, 2003.

54. Vallet, M., Vallade, M. and Berge, B., "Limiting phenomena for the spreading of water on polymer films by electrowetting by electrowetting," European Physical Journal, Vol. 11, No. 4, pp. 583-591, 1999.

55. Verheijen, H. J. J. and Prins, M. W. J., "Reversible electrowetting and trapping of charge: model and experiments," Langmuir, Vol. 15, No. 20, pp. 6616-6620, 1999.

56. Pollack, M. G., Fair, R. B. and Shenderov, A. D.,

"Electrowetting-based actuation of liquid droplets for microfluidic applications," Applied Physics Letters, Vol. 77, No. 11, pp. 1725-1726, 2000.

57. Pollack, M. G., Shenderov, A. D. and Fair, R. B., "Electrowetting-based actuation of droplets for integrated microfluidics," Lab on a Chip, Vol. 2, No. 2, pp. 96-101, 2002.
58. Ren, H., Fair, R. B., Pollack, M. G. and Shaughnessy, E. J., "Dynamics of electro-wetting droplet transport," Sensors and actuators B: chemical, Vol. 87, No. 1, pp. 201-206, 2002.
59. Daniel, S. and Chaudhury, M. K., "Rectified motion of liquid drops on gradient surfaces induced by vibration," Langmuir, Vol. 18, No. 9, pp. 3404-3407, 2002.
60. Extrand, C. W., "A thermodynamic model for contact angle hysteresis," Journal of Colloid and Interface Science, Vol. 207, No. 1, pp. 11-19, 1998.
61. Dickerson, R. E., Gray, H. B. and Haight, G. P., "Chemical Principles," W. A. Benjamin, Inc., 1974.
62. Furmidge, C. G. L., "Studies at phase interfaces I. The sliding of liquid drops on solid surfaces and a theory for spray retention," Journal of Colloid Science, Vol. 17, No. 4, pp. 309-324, 1962.
63. Latorre, L., Kim, J., Lee, J., de Guzman, P.-P., Lee, H. J., Nouet, P. and Kim, C.-J., "Electrostatic actuation of microscale liquid-metal droplets," Journal of Microelectromechanical Systems, Vol. 11, No. 4, pp. 302-308, 2002.
64. Smithwick, R. W. III, "Contact-angle studies of microscopic mercury droplets on glass," Journal of Colloid and Interface Science, Vol. 123, No. 2, pp. 482-485, 1988.
65. Chung, S. K., Zhao, Y. and Cho, S. K., "On-chip creation and elimination of microbubbles for micro-object manipulator," Journal of Micromechanics and Microengineering, Vol. 18, No. 9, Paper No. 095009, 2008.
66. Neagu, C., Gardeniers, J. G. E., Elwenspoek, M. and Kelly, J. J., "An electrochemical microactuator: principle and first results," Journal of Microelectromechanical Systems, Vol. 5, No. 1, pp. 2-9, 1996.
67. Leighton, T. G., "The Acoustic Bubble," Academic Press, 1997.
68. Tho, P., Manasseh, R. and Ooi, A., "Cavitation microstreaming patterns in single and multiple bubble systems," Journal of Fluid Mechanics, Vol. 576, pp. 191-233, 2007.
69. Marmottant, P. and Hilgenfeldt, S., "Controlled vesicle deformation and lysis by single oscillating bubbles," Nature, Vol. 423, No. 6936, pp. 153-156, 2003.
70. Marmottant, P., Raven, J. P., Gardeniers, H., Bomer, J. G. and Hilgenfeldt, S., "Microfluidics with ultrasound-driven bubbles," Journal of Fluid Mechanics, Vol. 568, pp. 109-118, 2006.
71. Ko, S. H., Lee, S. J. and Kang, K. H., "A synthetic jet produced by electrowetting-driven bubble oscillations in aqueous solution," Applied Physics Letters, Vol. 94, No. 19, Paper No. 194102, 2009.
72. Coakley, W. T. and Nyborg, W., "Cavitation; dynamics of gas bubbles; applications," Elsevier: New York, pp. 77-159, 1978.
73. Miller, D. L., "Particle gathering and microstreaming near ultrasonically activated gas-filled micropores," Journal of Acoustical Society of America, Vol. 84, No. 4, pp. 1378-1387, 1988.
74. Chung, S. K. and Cho, S. K., "3-D manipulation of millimeter- and micro-sized objects using an acoustically-excited oscillating bubble," Microfluidics and Nanofluidics, Vol. 6, No. 2, pp. 261-265, 2008.
75. Chung, S. K. and Cho, S. K., "Capturing, carrying, and releasing of micro-objects by AC-electrowetting-actuated oscillating bubbles," The 15th International Conference on Solid-State Sensors, Actuators and Microsystems (Transducers 2009), pp. 821-824, 2009.
76. Chung, S. K., Zhao, Y., Yi, U.-C. and Cho, S. K., "Micro bubble fluidics by EWOD and ultrasonic excitation for micro bubble tweezers," 20th International Conference on Micro Electro Mechanical Systems (MEMS), pp. 31-34, 2007.
77. Papavasiliou, A. P., "Bubble-actuated planar microvalves," Ph. D. Thesis, Department of Mechanical Engineering, University of California, Berkeley, pp. 1-118, 2001.
78. Suzuki, H. and Yoneyama, R., "A reversible electrochemical nanosyringe pump and some considerations to realize low-power consumption," Sensors and Actuators B: chemical, Vol. 86, No. 2-3, pp. 242-250, 2002.
79. Yang, S.-C. and Liu, C.-H., "An electrolysis-bubble-actuated micropump using electrowetting on dielectric (EWOD) for 1xN micro-sample switches," The 15th International Conference on Solid-State Sensors, Actuators and Microsystems (Transducers 2009), pp. 2018-2021, 2009.
80. Liu, R. H., Yang, J., Pindera, M. Z., Athavale, M. and Grodzinski, P., "Bubble-induced acoustic micromixing," Lab on a Chip, Vol. 2, No. 3, pp. 151-157, 2002.
81. Chung, S. K. and Cho, S. K., "Oscillating Mobile Bubbles for Microfluidic Mixing Enhancement," The 11th International Conference on Miniaturized Systems for Chemistry and Life Sciences (μTAS 2007), pp. 913-915, 2007.
82. Ryu, K., Chung, S. K. and Cho, S. K., "Separation and Collection of Microparticles Using Oscillating Bubbles," The 12th International Conference on Miniaturized Systems for Chemistry and Life Sciences (μTAS 2008), pp. 1471-1473, 2008.
83. Chung, S. K., Ryu, K. and Cho, S. K., "Electrowetting propulsion of water-floating objects," Applied Physics Letters,

Vol. 95, No. 1, Paper No. 014107, 2009.

84. Gao, X. and Jiang, L., "Biophysics: Water-repellent legs of water striders," Nature, Vol. 432, No. 7013, pp. 36-38, 2004.

85. Hu, D. L. and Bush, J. W. M., "Meniscus-climbing insects," Nature, Vol. 437, No. 7059, pp. 733-736, 2005.

86. Hu, D. L., Chan, B. and Bush, J. W. M., "The hydrodynamics of water strider locomotion," Nature, Vol. 424, No. 6949, pp. 663-666, 2003.

87. Lee, S. M., Oh, D. J., Jung, I. D., Bae, K. M., Jung, P. G., Chung, K. H., Cho, S.-J. and Ko, J. S., "Fabrication of Nickel Micromesh Sheets and Evaluation of their Water-repellent and Waterproof Abilities," Int. J. Precis. Eng. Manuf., Vol. 10, No. 3, pp. 161-166, 2009.

88. Song, Y. S. and Sitti, M., "Surface-Tension-Driven Biologically Inspired Water Strider Robots: Theory and Experiments," IEEE Transactions on robotics, Vol. 23, No. 3, pp. 578-589, 2007.

89. Mita, Y., Li, Y., Kubota, M., Parkes, W., Haworth, L. I., Flynn, B. W., Terry, J. G., Tang, T.-B., Ruthven, A. D., Smith, S. and Walton, A. J., "Demonstration of a wireless driven MEMS pond skater that uses EWOD technology," Solid-State Electronics, Vol. 53, No. 7, pp. 798-802, 2009.

90. Donald, B. R., Levey, C. G., McGray, C. D., Paprotny, I. and Rus, D., "An Untethered, Electrostatic, Globally Controllable MEMS Micro-Robot," Journal of Microelectromechanical Systems, Vol. 15, No. 1, pp. 1-15, 2006.

91. Jager, E. W. H., Inganäs, O. and Lundström, I., "Microrobots for Micrometer-Size Objects in Aqueous Media: Potential Tools for Single-Cell Manipulation," Science, Vol. 288, No. 5475, pp. 2335-2338, 2000.

92. Watson, B., Friend, J. and Yeo, L., "Piezoelectric ultrasonic resonant motor with stator diameter less than 250 μm: the Proteus motor," Journal of Micromechanics and Microengineering, Vol. 19, No. 2, Paper No. 022001, 2009.

93. Yesin, K. B., Vollmers, K. and Nelson, B. J., "Modeling and Control of Untethered Biomicrorobots in a Fluidic Environment Using Electromagnetic Fields," The International Journal of Robotics Research, Vol. 25, No. 5-6, pp. 527-536, 2006.

94. Zhang, L., Abbott, J. J., Dong, L., Kratochvil, B. E., Bell, D. and Nelson, B. J., "Artificial bacterial flagella: Fabrication and magnetic control," Applied Physics Letters, Vol. 94, No. 6, Paper No. 064107, 2009.

95. Cho, K.-J., Koh, J.-S., Kim, S., Chu, W.-S., Hong, Y. and Ahn, S.-H., "Review of Manufacturing Processes for Soft Biomimetic Robots," Int. J. Precis. Eng. Manuf., Vol. 10, No. 3, pp. 171-181, 2009.

96. Chung, S. K. and Cho, S. K., "Propulsion by Acoustically Excited Oscillating Bubbles for Biomedical Micro/Mini Robots Swimming Inside Human Body," The 13th International Conference on Miniaturized Systems for Chemistry and Life Sciences (μTAS 2009), pp. 1485-1487, 2009.

97. Ryu, K., Zueger, J., Chung, S. K. and Cho, S. K., "Underwater Propulsion Using AC-Electrowetting-Actuated Oscillating Bubbles for Swimming Robots," The 23st International Conference on Micro Electro Mechanical Systems (MEMS 2010), pp. 160-163, 2010.